Western University

Scholarship@Western

Chemistry Publications   Chemistry Department

6-2-2020

Benzosiloles with Crystallization-induced Emission Enhancement of Electrochemiluminescence: Synthesis, Electrochemistry, and Crystallography

Liuqing Yang

Donghyun Koo

Jackie Wu

Jonathan M. Wong

Tyler Day

See next page for additional authors

Follow this and additional works at: https://ir.lib.uwo.ca/chempub

⊕ Part of the Materials Chemistry Commons, Organic Chemistry Commons, and the Physical Chemistry Commons

Authors

Liuqing Yang, Donghyun Koo, Jackie Wu, Jonathan M. Wong, Tyler Day, Ruizhong Zhang, Harshana Kolongoda, Kehan Liu, Jian Wang, Zhifeng Ding, and Brian Pagenkopf

Benzosiloles with Crystallization-induced Emission Enhancement of Electrochemiluminescence: Synthesis, Electrochemistry, and Crystallography

Liuqing Yang[‖], Donghyun Koo[‖], Jackie Wu[‖], Jonathan M. Wong, Tyler Day, Ruizhong Zhang, Harshana Kolongoda, Kehan Liu, Jian Wang, Zhifeng Ding* and Brian L. Pagenkopf*

[a]   L. Yang[‖], D. Koo[‖], J. Wu[‖], J. M. Wong, T. Day, R. Zhang, H. Kolongoda, K. Liu, J. Wang, Prof. Dr. Z. Ding*, Prof. Dr. B. L. Pagenkopf*
       Department of Chemistry
       The University of Western Ontario
       1151 Richmond St., London, N6A 5B7, ON, Canada
       E-mail: zfding@uwo.ca (ZD); bpagenko@uwo.ca (BLP)

       [‖]Authors contributed equally

       Supporting information for this article is given via a link at the end of the document.

Abstract: Crystallization-induced emission enhancement (CIEE) was demonstrated for the first time for electrochemilunimescence (ECL) with two new benzosiloles. Compared with their solution, the films of the two benzosiloles gave CIEE of 24 times and 16 times. The mechanism of the CIEE-ECL was examined by spooling ECL spectroscopy, X-ray crystal structure analysis, photoluminescence, and DFT calculation. This CIEE-ECL system is a complement to the well-established aggregation-induced emission enhancement (AIEE) systems. Unique intermolecular interactions are noted in the crystalline chromophore. The first heterogeneous ECL system is established for organic compounds with highly hydrophobic properties.

Introduction

Electrogenerated chemiluminescence (ECL), also known as electrochemiluminescence, represents an important light-emitting process induced in the vicinity of working electrodes.[1] ECL can be produced via either the annihilation route (*i.e.*, the recombination of radical cations and anions of a luminophore) or the coreactant route (*i.e.*, an electrochemical reaction between a luminophore radical and a suitable coreactant).[2] ECL is increasingly employed in medical research, environmental monitoring, light-emitting devices, *etc.*[1-3] because of its advantages such as ease of control, low detection limit, high sensitivity, *etc.* Luminophores applied in an ECL system include organic molecules,[4] inorganic complexes,[5] and nanomaterials.[6] Currently, the most commonly employed ECL luminophore for different applications is ruthenium tris(2,2'-bipyridyl), *i.e.*, $Ru(bpy)_3^{2+}$. Additional ECL luminophores with good performance and low cost have always been avidly desired.

Highly π-conjugated compounds containing silole rings (1-silacyclopentadiene)[4a, 7] have been adopted for use in polymeric solar cells, electrochemiluminescent sensors, and light-emitting diodes.[8] The unique photophysical properties of siloles arise from their low-lying LUMO due to the σ*–π* conjugation between the π* orbital of the butadiene moiety and the σ* orbital of the two exocyclic σ-bonds on the silicon atom. We previously prepared 2,5-bis(arylethynyl)siloles and minimized non-emissive

decay processes by increasing the steric bulk on both the silicon atom and the 2,5-substituents to improve photoluminescence (PL) quantum efficiency.[7a, 9] Similarly, we demonstrated enhanced ECL from siloles by decorating them with 2,5-di(2-thienyl) substituents that are rich in π-electrons and by strategic steric tuning at the silicon atom.[4c] After these accomplishments, we chose to investigate 2-thienyl-benzo[*b*]siloles because (1) there is a rising interest in fused silole materials and (2) benzosiloles are synthetically well operable and expected, from theoretical calculations, to possess electrochemical properties superior than previously reported siloles including ours.[7a, 10] We were hence intrigued if we could improve the photoelectrochemical performance of benzosiloles similarly with the successful synthetic manipulation of steric and electronic properties previously applied to enhance siloles.

Tang found that some compounds are highly luminescent as aggregates/clusters but non-emissive or weakly emissive when molecularly dissolved in solution, and reported the aggregation-Induced emission (AIE).[11] The restriction of intramolecular motions such as rotation and vibration gives rise to the AIE property of these special molecules.[12] In a related content, crystallization-induced emission enhancement (CIEE) was also later reported by Tang[13] for hexaphenylsiloles and some other compounds whose light emission is remarkably stronger when they exist in the solid crystalline state compared with their amorphous or solution state. CIEE is undoubtedly desirable for light-emitting electrochemical cells, organic light-emitting diodes, *etc.*, since the layer responsible for light emission in these devices is usually a crystalline film. In fact, some reports adopted heterogeneous ECL to improve analytical performance,[4a, 6c, 14] but such a strategy is not readily feasible for existing organic ECL chromophores whose solid films are extreme hydrophobic and minimally wettable in aqueous systems but dissolve thoroughly in organic solvents.

Herein we report two newly developed chromophores, *i.e.*, 2-(2-thienyl)-benzo[*b*]silole (**4T1**) and 2-(2,2'-bithiophen)-5-yl]-benzo[*b*]silole (**4T2**) along with their electrochemistry and ECL in both annihilation and coreactant routes, with particular emphasis on the notably enhanced photoluminescence (PL) and ECL of

their crystalline films thanks to CIEE.[15] In fact, this is the first time that CIEE is invoked to describe ECL enhancement, and our observations and conclusions complement aggregation-induced electrochemiluminescence (AIECL), a topic recently reviewed by Xu for several compounds.[16]

Results and Discussion

Among the several available synthetic routes for benzosilole,[17] we chose to begin our synthesis with a double trimethylsilylation of the bromobenzonitrile **1** (Scheme 1).[18] Lithium halogen exchange followed by treatment with trimethylborate gave the boronic acid **2** (52% yield over three steps). Reaction of **2** with acetylene **3** (*n* = 1, 2) by rhodium(I)-catalyzed Chatani alkyne cycloaddition afforded the thienyl-appended benzosilole adducts **4T1** and **4T2** without any complication from the nitrile.[19] Mechanistic studies suggest that extremely harsh conditions are needed to cleave the C(alkyl)–Si bond.[20] In contrast, in the Chatani reaction, a Rh(I)-mediated activation process gives the annulative coupling products **4T1** and **4T2** under relatively mild conditions with 63% and 54% yield, respectively.
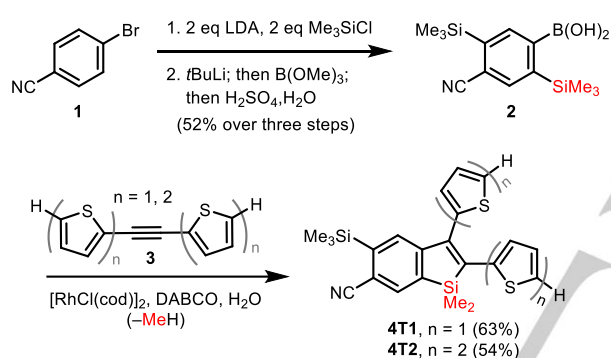
Scheme 1. Synthesis of benzosiloles **4T1** and **4T2**. LDA = lithium diiso-propylamide, cod = cyclooctadiene, DABCO = 1,4-diazabicyclo[2.2.2]octane.

Figure 1A shows the cyclic voltammograms (CVs, grey curve) of 0.5 mM **4T2** in dichloromethane (DCM) with 0.1 M tetrabutylammonium perchlorate (TBAP) as the supporting electrolyte. When the potential was scanned positively, **4T2** underwent three oxidation reactions to produce its radical cation at 1.12 V, dication at 1.90 V, and radical trication at 2.20 V, respectively. In contrast, only one reduction peak was observed at −1.99 V in the cathodic scan. DFT calculations visualize the electron density across the frontier molecular orbitals in the electronic structure of **4T2** (inset of Figure 1A). Specifically, the electrons in the HOMO are well delocalized across a conjugated system that encompasses the silole, the aryl group, and the bithiophenyl group at the α-position of the silole ring, whereas the electrons in the LUMO are mainly spread over the benzosilole core. Note that neither the HOMO nor the LUMO shows electrons across the β-bithiophenyl. Without doubt, the oxidation took place in the conjugated system whereas the reduction occurred mainly within the benzosilole moiety. The electrochemistry of **4T1** (Figure S1) reveals two oxidation waves and one reduction wave at 1.18, 1.67, and −1.84 V, respectively. It is speculated that because **4T2** has one more thiophene unit, the extended conjugation and coplanarity of the benzosilole and bithiophenyl moieties in **4T2** facilitate the oxidation reactions

compared with those of **4T1**. The observed redox potentials agree well with DFT calculation results (Figure 1A).

Figure 1A also displays the ECL–voltage curve (green curve) corresponding to the CV described above. Both the first and second oxidation peaks of **4T2** exhibit ECL, but no ECL was found in the cathodic scan, and **4T1** has only one cathodic ECL signal (Figure S1A). For **4T2**, the generally proposed mechanism of the first ECL peak[1-2] involves the reaction between radical cations and anions, the production of excited states, and the radiative relaxation of the excited states with light emission. The second ECL wave (3 nA) is stronger than the first (0.8 nA) because of the formation of the **4T2** dication, which can be rationalized as follows: The transfer of one electron in the HOMO of neutral **4T2** to the LUMO of the **4T2** dication produces two radical cations to thus increase the intensity of the second ECL (inset scheme in Figure 1A). The maximum ECL intensity of **4T2** reached 3 nA. When $Ru(bpy)_3(PF_6)_2$ of the same concentration was used as the reference, the ECL efficiency of **4T2** and **4T1** was calculated to be 2.3% and 2.1%, respectively.
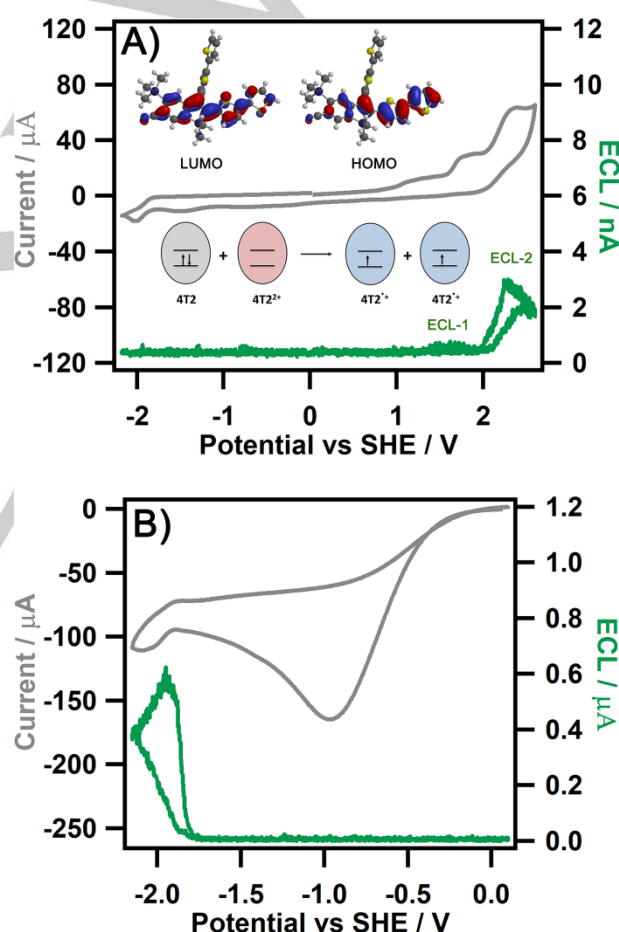
Figure 1. Cyclic voltammograms (CVs, grey) of 0.5 mM **4T2** in DCM at a scan rate of 0.1 V/s with 0.1 M TPAP as the supporting electrolyte (A) scanning to both positive and negative potentials in the absence of 5 mM BPO, and (B) scanning only to negative potential in the presence of 5 mM BPO. Insets in (A) are the molecular orbitals iso-surface plots for the HOMO and LUMO of **4T2** based on the DFT/B3LYP/6-31G* calculations. The ECL voltage curves are overlaid at the bottom in green.

We then added benzoyl peroxide (BPO) as an oxidizing coreactant to improve the observed low ECL signal (Figures 1A

and S1A) from the annihilation route of both **4T2** and **4T1**. In the presence of 5 mM BPO, the ECL intensity of **4T2** was enhanced significantly to ~550 nA (Figure 1B), but this coreactant ECL process gives a low ECL efficiency of 0.4% when the $Ru(bpy)_3(PF_6)_2$/BPO coreactant system was used as the benchmark. When the voltage was pulsed at 10 Hz between 0.10 V and the cathodic potential limit (−2.40 V), the ECL intensity of **4T2** reached ~3 µA (Figure S2A). The pulsing experiment changed the applied potential rapidly enough to decrease the time for the electrochemically generated silole radicals to decay, and the ECL intensity thus became much higher. For **4T1** with 5 mM BPO, the ECL intensity was increased to 120 nA in potential scanning and to 400 nA in pulsing, but the **4T1**/BPO system has an even lower ECL efficiency of 0.08% based on $Ru(bpy)_3(PF_6)_2$/BPO.

Figure 2A displays the spooling ECL spectra of the above **4T2**/BPO coreactant system acquired with a potential scanning cycle between 0.10 V and −2.10 V, in which the two ECL features are color-labeled in orange (−1.70 V to −1.98 V) and purple (−1.98 V to −1.68 V), respectively. The wavelength of the ECL emission peak is at 630 nm throughout the scan, which is redshifted from the PL at 475 nm (Table 1). This huge difference is ascribed to the drastically different excited states of the PL (monomer excited states) and ECL processes (dimer excited states, excimer).
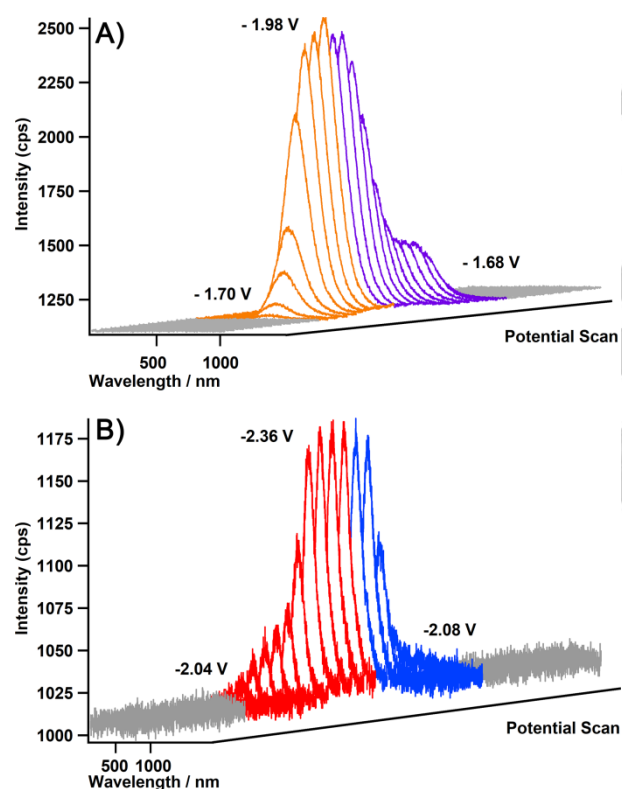

Figure 2. Spooling ECL spectra of 0.5 mM (A) **4T2** and (B) **4T1** in DCM in the presence of 5 mM BPO at 0.02 V/s scan rate with 2 s accumulation time for each spectrum.

Table 1. PL and ECL peak wavelength and ECL efficiency for both **4T1** and **4T2** in solution and crystal solid state.

	PL Peak Wavelength	ECL Peak Wavelength	ECL Efficiency
4T1 solution	428 nm	602 nm	0.08%
4T1 crystal film	533 nm	528 nm	2.5%
4T2 solution	475 nm	630 nm	0.4%
4T2 crystal film	602 nm	607 nm	6.5%

Two possible mechanisms of excimer generation in the ECL route are considered. For both, at around −0.80 V, BPO is firstly reduced to generate a benzoate radical (PhCOO•), which then oxidizes **4T2** to produce **4T2**•+. In the first mechanism, at about −1.70 V, excess neutral **4T2** is reduced to **4T2**•−, which then reacts with **4T2**•+ to generate a dimer as the excimer to emit ECL. In the second mechanism, after **4T2**•+ is generated from the oxidation by PhCOO•, a typical electrochemical dimerization can occur[21] at the thiophene units in **4T2** to produce a ground state dimer, and the ground state dimer then reacts with BPO to become the excimer via a classical ECL reaction. In the pulsing experiment, the applied potential is alternated very quickly, and the ECL would not improve if a slow electrochemical process such as the generation of ground state dimer[21] is involved. Hence, the observed ECL enhancement by pulsing effectively rules out the second mechanism. The solution ECL here has to have the first mechanism because the emission wavelength in the spooling spectrum shows only the dimer and no monomer as the excimer. At −1.70 V, the potential is high enough to produce both the radical species of the **4T2** dimer and the BPO radical. As the cathodic scan continues, the increasingly negative potential generates a greater number of radical species, and the ECL intensity thus escalates and peaks at −1.98 V. When the voltage is applied in the reverse direction, the ECL intensity decreases due to the reverse reaction between the **4T2** dimer and the BPO radical species before ECL disappears at −1.68 V. The ECL behaviors from real-time spooling match well with the ECL–voltage curve in Figure 1B. The ECL peak of **4T1** at 602 nm also has a redshift of 174 nm from the PL at 428 nm (Table 1, Figure 2B).

After recording the low ECL efficiency of **4T2** and **4T1** in solution, we dropcast them to prepare a film for each on glassy carbon working electrodes to assess the ECL performance from the resulting crystal filmed-electrodes. Gratifyingly, upon irradiation at 254 nm, the crystal film of **4T2** on the electrode gave an orange emission and the crystal film of **4T1** gave a green emission (insets in Figure 3A,B). Additional experiments were carried out to verify the solid films on the electrodes are indeed crystalline. We firstly recrystallized **4T2** and carefully transferred the crystals to a mortar. At this point, the crystals gave off an orange color both in daylight (Figure 4A) and under 254 nm UV (Figure 4B). The crystals were then ground with a pestle[22] to give amorphous **4T2**, which then showed not an orange color but a yellow color both in daylight (Figure 4D) and under 254 nm UV (Figure 4E). Additionally, we dropcast the DCM solution of **4T2** on a piece of quartz glass and also deposited the solution on a TLC plate (Figure 4C). On the quartz glass, **4T2** remained in its crystalline state[13c, 23] and gave the same orange color. In contrast, the **4T2** dispersed in the silica gel matrix became amorphous,[13c] and the observed color became yellow (Figure 4F). Therefore, the thin film of **4T2** on the glassy carbon
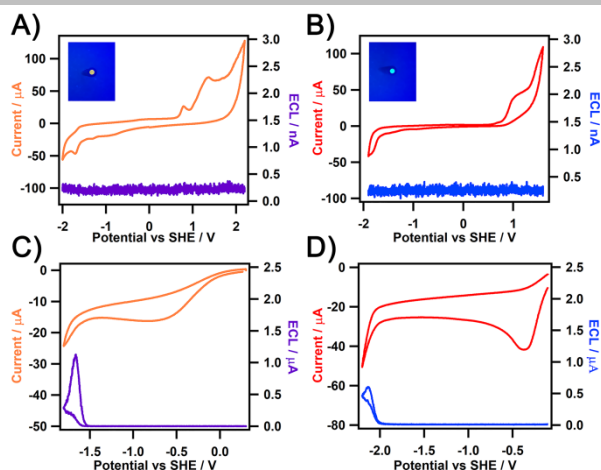
Figure 3. Cyclic voltammogram at 0.1 V/s scan rate of (A) **4T2** films in annihilation route, (B) **4T1** films in annihilation route, (C) **4T2** films with 5 mM BPO as coreactant, and (D) **4T1** films with 5 mM BPO as coreactant. The insets of (A) and (B) are the crystal films of **4T2** and **4T1** modified on glassy carbon electrodes under UV 254 nm irradiation, respectively. The ECL voltage curves are overlaid at the bottom in purple (A and C) and blue (B and D).
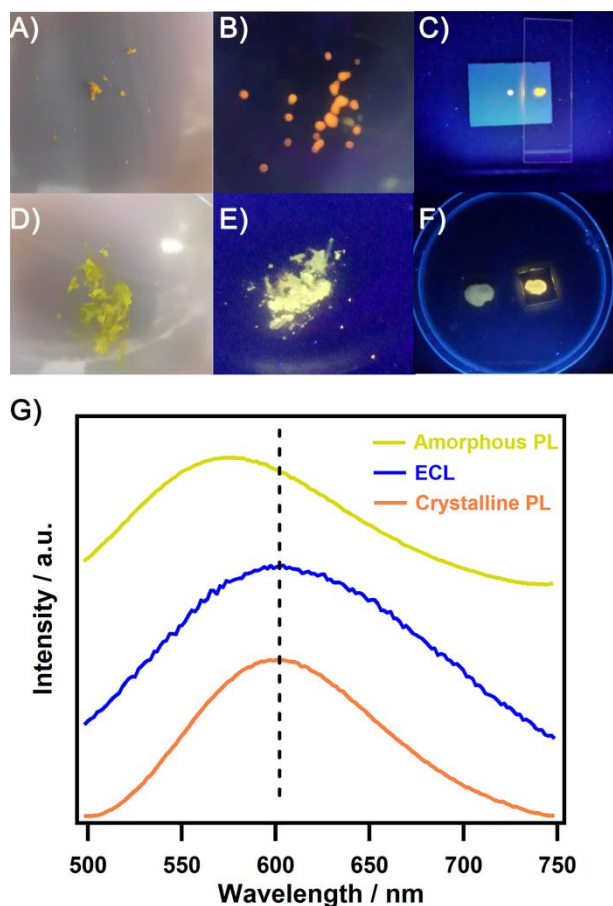

Figure 4. 4T2 crystals under daylight (A) and under 254 nm irradiation (B). (C) Amorphous **4T2** on TLC plate (left) and crystalline **4T2** on quartz (right). Amorphous **4T2** under daylight (D) and under 254 nm irradiation (E). (F) Amorphous **4T2** in silica gel matrix (left) and crystalline **4T2** on quartz (right). (G) PL spectra of amorphous (gold) and crystalline (orange) **4T2** along with ECL spectrum of a crystal film electrode in contact with 5 mM BPO in water/acetonitrile electrolyte solution.

electrode exhibits crystalline property because the electrode displays an orange color under UV irradiation (inset of Figure 3A).

Testing the ECL of the filmed-electrode requires a careful selection of the solvent. The solvent needs to be able to make intimate conductive contact with the film surface while not dissolving the film. DCM easily dissolves the films of **4T1** and **4T2** and clearly cannot be used. Although aqueous systems are widely reported,[4a, 6c, 14] the films of **4T1** and **4T2** are highly hydrophobic and show no electrochemical or ECL behavior in purely aqueous system (Figure S3). After screening a number of common solvents for electrochemistry and ECL compatibility, we found that the films have relatively poor solubility in acetonitrile, although they are not yet insoluble enough in acetonitrile (see ECL results in Figure S4). Eventually, the filmed-electrode ECL of **4T1** and **4T2** was assessed in 1:1 v/v water/acetonitrile.

Figure 3A,B shows the CV and ECL–voltage curves of **4T2** and **4T1** crystal films in 1:1 v/v water/acetonitrile containing 0.1 M tetramethylammonium perchlorate (TMAP) as the supporting electrolyte. Although the shapes of the peaks seem somewhat different, **4T2** crystal films also display three oxidations and one reduction, and **4T1** films also show two oxidations and one reduction, both in agreement with the observations of the **4T2** and **4T1** solutions. No ECL was observed in the annihilation route for the films because they are subject to surface effect.[24] Specifically, when **4T2** and **4T1** are prepared as crystalline thin films, the electrochemical and luminescent behaviors become restricted because their radical species are no longer available in solution. In contrast, the solution ECL is related to the concentration change of reactive species in the vicinity of the working electrode and thus can readily occur via annihilation.[24]

The addition of 5 mM BPO into the solution greatly enhanced the ECL of the filmed electrodes (Figure 3C,D), with the **4T2** system giving nearly 1.1 µA and the **4T1** system 600 nA. The ECL intensity became even stronger in the pulsing experiments (Figure S5), giving 4 µA for **4T2** and 1 µA for **4T1**, respectively. The accumulation ECL spectrum of the **4T2** film shows peak wavelength at 607 nm (Figure 4G), which is now almost the same as the PL peak of the **4T2** crystal (602 nm, Figure 4G and Table 1). Because the film dropcast on the glassy-carbon electrodes is verified to be crystalline (Figure 4G), the crystals must have the same excited states in both PL and ECL process. The PL experiments of the solid films were conducted using the same spectrometer for ECL along with a 405 nm laser excitation source. Compared with the solution PL, the crystalline PL signals of **4T1** and **4T2** are both significantly enhanced and strongly redshifted (insets of Figure 5). Figure 5 shows spooling ECL spectra of the filmed electrode with (A) **4T2** and (B) **4T1** in the presence of 5 mM BPO, which depict the same peak wavelength for each compound during ECL evolution and devolution. It is evident by the spooling ECL spectroscopy that both **4T2** and **4T1** possess only one excited state each.

A single crystal suitable for X-ray analysis was harvested from the DCM solution of **4T2**. In the X-ray structure of **4T2** (Figure 6A), the benzosilole core and the phenyl group resides in the same plane along with the α-bithiophenyl group. That is, **4T2** has a highly conjugated system consisting of these three parts. Note that the bithiophenyl group at the β-position of the silole is twisted away from the conjugated system (see discussion

below). Hence, redox reactions happen in the conjugated system but not the β-bithiophenyl, as is also seen from the DFT calculations (inset of Figure 1A).
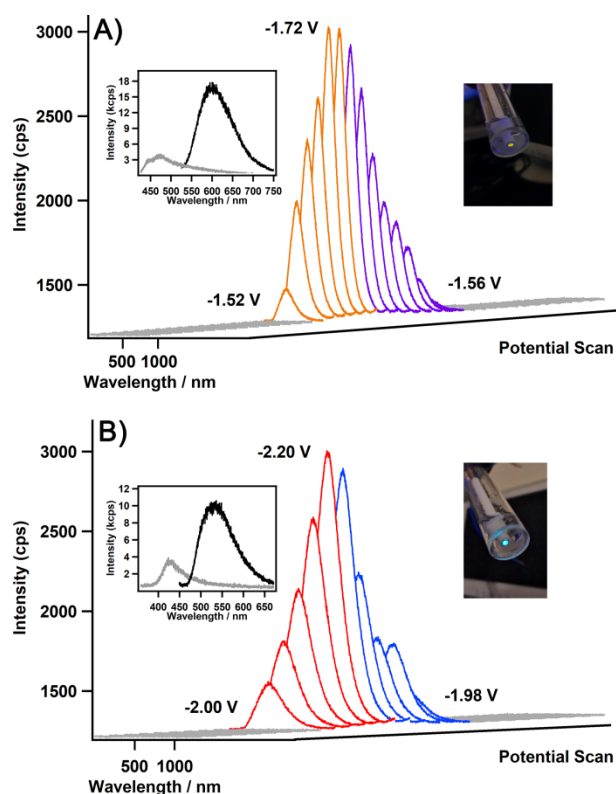

Figure 5. Spooling ECL spectra of the filmed electrode with (A) **4T2** and (B) **4T1** in the presence of 5 mM BPO at a scan rate of 0.02 V/s and exposure time of 2 s. Insets on the left in both (A) and (B) are the PL spectra of **4T2** in solution (grey) and solid state (black). Insets on the right in both (A) and (B) display the photo of the electrochemical cell used for the ECL experiment under the UV irradiation (265 nm).
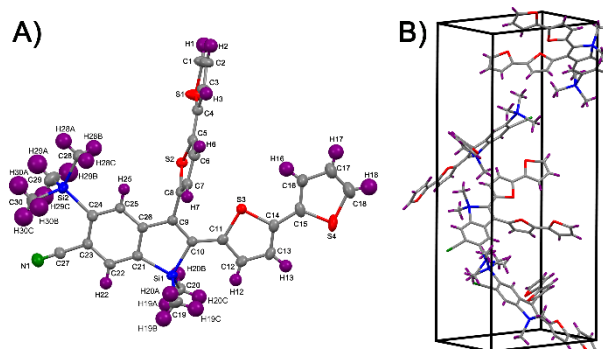

Figure 6. X-ray crystal structures of **4T2**: (A) single molecule, (B) within the packing system. The dichloromethane solvent molecule is removed for clarity.

The conformations of **4T1** and **4T2** in solution are illustrated in the insets of Figure 1A. The PL emission of **4T1** and **4T2** is less pronounced in solution because the excited states can be deactivated nonradiatively by various intramolecular motions (e.g., rotation of the bonds between the silole core and the thiophenyl/bithiophenyl group). In contrast, a number of restrictions on the conformational freedom can be noted for the crystalline structure of **4T2**. Although conventional forces like

hydrogen bonding and π-π stacking, key factors for CIEE,[15] are both lacking in the **4T2** molecule, conformation rigidification is still noted for **4T2** and established unambiguously from several intriguing intermolecular interactions (Figure 7). For example, the hydrogen atom (H18, electron-deficient) at the far end of the α-bithiophenyl group seems to have an electrostatic interaction with the β-bithiophenyl group (C3 and C4 in the thiophene ring containing S1, electron-rich) in the neighboring benzosilole (Figure 7A, Table 2), and this interaction presumably helps enhance the properties of **4T2** in comparison with **4T1**. Besides, the nitrogen atom on the 4-cyano substituent of **4T2** is also affected by the β-bithiophenyl moiety (interaction between N1 and the H6 atom on the thiophene containing S3, Figure 7B, Table 2). In addition, the methyl groups on the Si atom seem to sterically restrain the rotation of the thiophene ring in the neighboring **4T2** molecule through two independent steric obstructions (Figure 7C,D, Table 2). Lastly, interaction is also noted between the proximal thiophene (S3) in the α-bithiophenyl and the distal thiophene (S1) in the β-bithiophenyl (Figure 7E, Table 2). All these intermolecular interactions contribute to the conformation rigidification of **4T2** crystal and enhance the PL emission. The dihedral angle between intersecting benzosilole planes in **4T2** is 98.91° (Figure S8), which clearly indicates J-aggregation (Figure 8). The 3-bithiophene moiety intersects the conjugated benzosilole within the same molecule at 99.60° and the neighboring benzosilole at 125.50°, respectively (Figure S8). The **4T2** crystalline film has a relative PL quantum yield of nearly 6%, about three times that of **4T2** in solution (2%). It is also
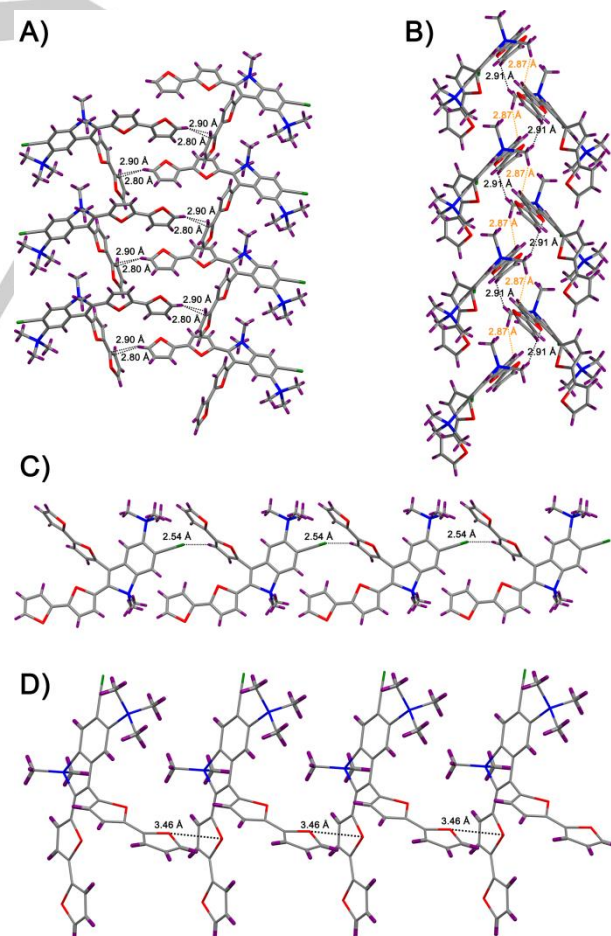

Figure 7. Intermolecular interactions in crystalline **4T2**. (A) H-π interaction between H18 and C2=C3. (B) Interaction between H6 and N1. (C) Interaction between S1 and S3. (D) Steric hindrance between H20 and C13. (E) Steric hindrance between H20 and S3.
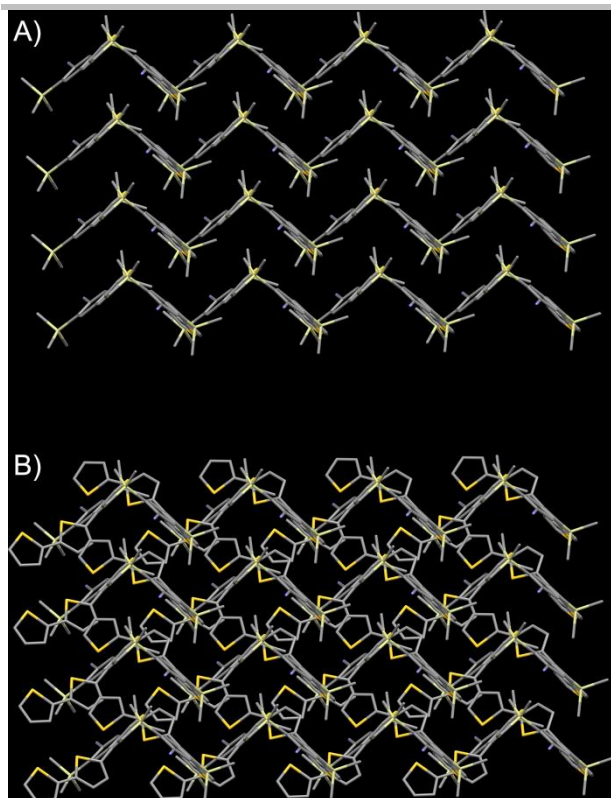
Figure 8. Illustration of J-aggregation of **4T2** with the β-bithiophene (a) hidden and (b) visualized.

recently summarized by Xu[16] has been reported for 1,1'-disubstituted 2,3,4,5-tetraphenylsiloles,[4a] carboranyl carbazoles,[14] tetraphenylethylene nanocrystals,[26] and platinum complexes,[27] but the performance difference between amorphous aggregate and crystalline film states has not been clearly shown prior to this report on benzosiloles. Is CIEE-ECL just an example of a well-ordered aggregate? We contend that CIEE-ECL should not be considered equivalent to AIECL, but rather it should be seen as an essential complement to AIECL. In the present case, ECL enhancement differs for electrodes modified with luminophores that exist as crystalline films or amorphous aggregates, and differentiating the ECL outcome can be simplified by invoking CIEE-ECL for crystalline films.

Table 2. Short contacts in the crystal structure of **4T2**.

Short Contact	Atom 1[a]	Atom 2[a]	Length[b]	Length−VdW[b]
#1[c]	H18	C3	2.797	−0.103
	H18	C4	2.897	−0.003
#2	H6	N1	2.538	−0.212
#3	H20	C13	2.867	−0.033
	H20	S3	2.913	−0.087
#4	S1	S3	3.459	−0.141

[a] Atoms numbered as in ORTEP (Figure 6A). [b] Length given in Å. [c] The dihedral angle between the S1 thiophene ring and the nearly isosceles triangle consisting of C3, C4, and H18 is 88.62°. The dihedral angle between the S4 and S1 thiophene rings is 61.21°. The length of the bond between C3 and C4 is 1.374 Å. The altitude from H18 to the base of the triangle (from C3 to C4) is calculated based on the law of cosines to be 2.756 Å.

reported that the interactions of chromophores can split the excited states into two energy levels. As for the case of J-aggregation which was revealed in 4T2 with twisted structure and bulky groups (Figure 8), the excitation was from the ground state to the lower energy level thus produces a redshifted PL emission (~80 nm in the case of **4T2** from solution to crystal).[25]

It is worth commenting that the ECL efficiency of the **4T2** film reaches 6.5% and is 16 times that of the **4T2** solution. The ECL efficiency of the **4T1** film also increases by 24 times compared with that of the **4T1** solution in DCM. That is, when the films of **4T2** and **4T1** are used instead of their solution, both the ECL intensity and the ECL efficiency improve greatly due to CIEE, a phenomenon previously reported by Tang for PL but never illustrated for ECL until the current work (see disambiguation between CIEE and AIEE below).[13c, 15] The solid crystal films of **4T2** and **4T1** have a rigid molecular packing (Figure 2B) that prohibits intramolecular rotations, diminishes nonradiative relaxation, and boosts the PL and ECL.[13c, 15] In contrast, in solution, the electrochemically generated excited states of **4T2** and **4T1** mainly return to the ground state by nonradiative relaxation via single bond rotations of the benzosilole–thiophene and thiophene–thiophene units, which seriously weaken the emissive process.

For the films ECL is not feasible via the annihilation route, but their ECL performance in the coreactant system vastly outperforms the solutions because ECL reactions occur at the interface between the benzosilole crystalline film and the water/acetonitrile solution, instead of only within the film as in the annihilation route. To the best of our knowledge, this is the first example where the ECL performance is demonstrated to improve significantly by CIEE. Previously, aggregation-induced emission enhancement (AIEE) of ECL, also known as AIECL, as

Conclusion

In summary, photoluminescence and ECL enhancement of two benzosiloles have been induced by crystallization, and was revealed by spooling ECL spectroscopy, X-ray crystallography, photoluminescence, and DFT calculation. The CIEE-ECL system is simple to design and convenient to use. Additionally, this work establishes a heterogeneous ECL performing system for highly hydrophobic organic compounds, and showcases the CIEE strategy to greatly enhance ECL intensity. Our experimental results complement aggregation-induced electrochemiluminescence (AIECL) and provide a platform for designing and processing more efficient optoelectronic devices.

Acknowledgements

[1] W. Miao, *Chem. Rev.* **2008**, *108*, 2506-2553.

[2] M. Hesari, Z. F. Ding, *J. Electrochem. Soc.* **2016**, *163*, H3116-H3131.

[3] a) M. M. Richter, *Chem. Rev.* **2004**, *104*, 3003-3036; b) L. Li, Y. Chen, J. J. Zhu, *Anal. Chem.* **2017**, *89*, 358-371.

[4] a) Z. Han, Z. Yang, H. Sun, Y. Xu, X. Ma, D. Shan, J. Chen, S. Huo, Z. Zhang, P. Du, X. Lu, *Angew. Chem. Int. Ed.* **2019**, *58*, 5915-5919; b) R. Zhang, F. Tong, L. Yang, J. R. Adsetts, T. Yan, R. Wang, Z. Ding, H. B. Wang, *Chem. Commun.* **2018**, *54*, 9897-9900; c) C. Booker, X. Wang, S. Haroun, J. Zhou, M. Jennings, B. L. Pagenkopf, Z. Ding, *Angew. Chem. Int. Ed.* **2008**, *47*, 7731-7735.

[5] a) S. Ladouceur, K. N. Swanick, S. Gallagher-Duval, Z. F. Ding, E. Zysman-Colman, *Eur. J. Inorg. Chem.* **2013**, *2013*, 5329-5343; b) K. N. Swanick, S. Ladouceur, E. Zysman-Colman, Z. Ding, *Angew. Chem. Int. Ed.* **2012**, *51*, 11079-11082; c) K. N. Swanick, M. Sandroni, Z. Ding, E. Zysman-Colman, *Chem. Eur. J.* **2015**, *21*, 7435-7440.

[6] a) M. Hesari, Z. Ding, *Acc. Chem. Res.* **2017**, *50*, 218-230; b) M. Hesari, M. S. Workentin, Z. Ding, *Chem. Eur. J.* **2014**, *20*, 15116-15121; c) R. Z. Zhang, J. R. Adsetts, Y. T. Nie, X. H. Sun, Z. F. Ding, *Carbon* **2018**, *129*, 45-53.

[7] a) A. J. Boydston, B. L. Pagenkopf, *Angew. Chem. Int. Ed.* **2004**, *43*, 6336-6338; b) H. Kinoshita, H. Fukumoto, A. Ueda, K. Miura, *Tetrahedron* **2018**, *74*, 1632-1645; c) V. Malytskyi, J. J. Simon, L. Patrone, J. M. Raimundo, *RSC Adv.* **2015**, *5*, 354-397.

[8] a) Y. J. Cai, A. J. Qin, B. Z. Tang, *J. Mater. Chem. C.* **2017**, *5*, 7375-7389; b)Y. Feng, C. Dai, J. Lei, H. Ju, Y. Cheng, *Anal. Chem.* **2016**, *88*, 845-850.

[9] E. Zhao, J. W. Y. Lam, Y. Hong, J. Liu, Q. Peng, J. Hao, H. H. Y. Sung, I. D. Williams, B. Z. Tang, *J. Mater. Chem. C.* **2013**, *1*, 5661.

[10] a) R. V. Solomon, A. P. Bella, S. A. Vedha, P. Venuvanalingam, *Phys. Chem. Chem. Phys.* **2012**, *14*, 14229-14237; b)Z. Y. Yu, Y. Lan, *J. Org. Chem.* **2013**, *78*, 11501-11507; c) F. B. Zhang, Y. Adachi, Y. Ooyama, J. Ohshita, *Organometallics* **2016**, *35*, 2327-2332; d) L. Xu, S. Zhang, P. F. Li, *Org. Chem. Front.* **2015**, *2*, 459-463; e)Q. W. Zhang, K. An, W. He, *Synlett* **2015**, *26*, 1145-1152.

[11] J. Luo, Z. Xie, J. W. Lam, L. Cheng, H. Chen, C. Qiu, H. S. Kwok, X. Zhan, Y. Liu, D. Zhu, B. Z. Tang, *Chem. Commun.* **2001**, 1740-1741.

[12] D. Wang, B. Z. Tang, *Acc. Chem. Res.* **2019**, *52*, 2559-2570.

[13] a) Y. Q. Dong, J. W. Y. Lam, Z. Li, A. J. Qin, H. Tong, Y. P. Dong, X. D. Feng, B. Z. Tang, *J. Inorg. Organomet. Polym. Mater.* **2005**, *15*, 287-291; b) J. W. Chen, C. C. W. Law, J. W. Y. Lam, Y. P. Dong, S. M. F. Lo, I. D. Williams, D. B. Zhu, B. Z. Tang, *Chem. Mater.* **2003**, *15*, 1535-1546; c) Y. Dong, J. W. Lam, A. Qin, Z. Li, J. Sun, H. H. Sung, I. D. Williams, B. Z. Tang, *Chem. Commun.* **2007**, 40-42.

[14] X. Wei, M. J. Zhu, Z. Cheng, M. Lee, H. Yan, C. Lu, J. J. Xu, *Angew. Chem. Int. Ed.* **2019**, *58*, 3162-3166.

[15] Y. Gong, L. Zhao, Q. Peng, D. Fan, W. Z. Yuan, Y. Zhang, B. Z. Tang, *Chem. Sci.* **2015**, *6*, 4438-4444.

[16] X. Wei, M. J. Zhu, H. Yan, C. Lu, J. J. Xu, *Chem. Eur. J.* **2019**, *25*, 12671-12683.

[17] a) J. Dubac, A. Laporterie, G. Manuel, *Chem. Rev.* **1990**, *90*, 215-263; b)H. Kinoshita, A. Ueda, H. Fukumoto, K. Miura, *Org. Lett.* **2017**, *19*, 882-885.

[18] S. Lulinski, J. Serwatowski, *J. Org. Chem.* **2003**, *68*, 5384-5387.

[19] M. Tobisu, Y. Kita, Y. Ano, N. Chatani, *J. Am. Chem. Soc.* **2008**, *130*, 15982-15989.

[20] a) M. Onoe, K. Baba, Y. Kim, Y. Kita, M. Tobisu, N. Chatani, *J. Am. Chem. Soc.* **2012**, *134*, 19477-19488; b) M. Tobisu, M. Onoe, Y. Kita, N. Chatani, *J. Am. Chem. Soc.* **2009**, *131*, 7506-7507.

[21] S. L. Meisel, G. C. Johnson, H. D. Hartough, *J. Am. Chem. Soc.* **1950**, *72*, 1910-1912.

[22] a) Z. Chen, J. Zhang, M. Song, J. Yin, G. A. Yu, S. H. Liu, *Chem. Commun.* **2015**, *51*, 326-329; b) P. Galer, R. C. Korosec, M. Vidmar, B. Sket, *J. Am. Chem. Soc.* **2014**, *136*, 7383-7394; c) B. Xu, M. Xie, J. He, B. Xu, Z. Chi, W. Tian, L. Jiang, F. Zhao, S. Liu, Y. Zhang, Z. Xu, J. Xu, *Chem. Commun.* **2013**, *49*, 273-275;

d) R. Zheng, X. F. Mei, Z. H. Lin, Y. Zhao, H. M. Yao, W. Lv, Q. D. Ling, *J. Mater. Chem. C.* **2015**, *3*, 10242-10248.

[23] M. Yamauchi, K. Yokoyama, N. Aratani, H. Yamada, S. Masuo, *Angew. Chem. Int. Ed.* **2019**, *58*, 14173-14178.

[24] A. J. Bard, Z. F. Ding, N. Myung, *Struct. Bond.* **2005**, *118*, 1-57.

[25] a) B. K. An, S. K. Kwon, S. D. Jung, S. Y. Park, *J. Am. Chem. Soc.* **2002**, *124*, 14410-14415; b) E. Da Como, M. A. Loi, M. Murgia, R. Zamboni, M. Muccini, *J. Am. Chem. Soc.* **2006**, *128*, 4277-4281; c) A. B. Koren, M. D. Curtis, A. H. Francis, J. W. Kampf, *J. Am. Chem. Soc.* **2003**, *125*, 5040-5050; d) Y. L. Wang, T. L. Liu, L. Y. Bu, J. F. Li, C. Yang, X. J. Li, Y. Tao, W. J. Yang, *J. Phys. Chem. C* **2012**, *116*, 15576-15583.

[26] J. L. Liu, J. Q. Zhang, Z. L. Tang, Y. Zhuo, Y. Q. Chai, R. Yuan, *Chem. Sci.* **2019**, *10*, 4497-4501.

[27] S. Carrara, A. Aliprandi, C. F. Hogan, L. De Cola, *J. Am. Chem. Soc.* **2017**, *139*, 14605-14610.

Entry for the Table of Contents
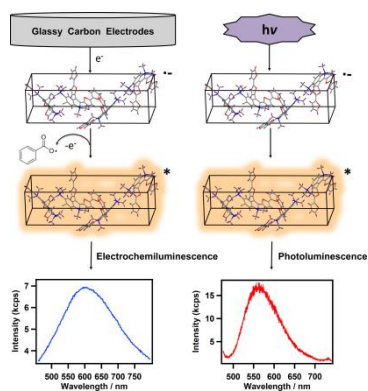
The photoluminescence and electrochemiluminescence (ECL) of two benzosiloles are significantly enhanced upon their crystallization. The developed ECL system with crystallization-induced emission enhancement is clearly differentiated from ECL systems with aggregation-induced emission enhancement, and it is also anticipated to find applications in ECL sensing and optoelectronics.